Revista Virtual de Química

Article

http://dx.doi.org/10.21577/1984-6835.20250038

Electrodeposition Process of Cobalt Films on Different Gold Substrates

Processo de Eletrodeposição de Filmes de Cobalto em Diferentes Substratos de Ouro

Deyse Melo Santos,[a] *Wladimir Hernandez Flores,*[a] *André Gündel*,*[a]

[a]Universidade Federal do Pampa, Campus Bagé, Zip Code 96413-170, Bagé-RS, Brazil

***E-mail:** andregundel@unipampa.edu.br

Submissão: 18 de Setembro de 2024

Aceite: 3 de Julho de 2025

Publicado online: 29 de Julho de 2025

This work investigates the electrodeposition process of thin cobalt films on three different gold substrates: CDtrode, Au/Mica, and Au/Silicon. The primary focus is on studying deposition mechanisms through the variation of the scan rate in cyclic voltammograms. Cyclic voltammetry tests were conducted, and the data obtained by varying the scan rate showed an increase in cobalt deposition and dissolution areas. A linear dependence of the peak current on the square root of the scan rate was observed, indicating that the process was quasi-reversible and diffusion-controlled. The cobalt oxidation process on the substrate surfaces was diffusion-controlled, according to the log Ip *versus* log v plot. The Au/Mica substrate showed a higher reduction peak current than the other substrates, indicating that its catalytic activity was higher, and that it likely had more active sites available for the reduction of cobalt II ions to be consumed at the substrate/electrolyte interface. However, the substrates showed promising results for future work on cobalt film electrodeposition. The study of thin cobalt films is of great importance in various fields of science and technology, primarily due to their magnetic and electronic properties. They have applications in magnetic storage, sensors, spintronics, and as catalysts in various chemical reactions.

Keywords: Cobalt thin films; cyclic voltammetry; electrodeposition; gold substrates; electrochemical characterization.

1. Introduction

In recent decades, magnetic thin films have generated great interest in modern microelectronics and spintronics applications because they have been successfully used in a wide variety of applications such as magnetic storage, spintronic devices, and magneto-optical switches.[1-3] Many of these films can be produced by physical deposition techniques such as molecular beam epitaxy (MBE),[4,5,6] physical vapor deposition (PVD), sputtering,[6,7] vacuum evaporation,[8,9] and pulsed laser deposition (PLD).[6,10]

However, these techniques have disadvantages, such as an appropriate cooling system for processes operating at high vacuum and temperature, the evaporation of materials with high melting points, need for skilled operators, and high production costs. Additionally, the deposition rate of the coatings is often low.[11] All these issues can be simplified using chemical deposition techniques such as metal-organic chemical vapor deposition (MOCVD),[12,13] atomic layer deposition (ALD),[14] and electrodeposition.[15,16] Among the various techniques for film deposition, electrodeposition is considered highly attractive because it is a simple, reliable, cost-effective, and extremely versatile method, along with other significant advantages.[15,16,17]

Cyclic voltammetry (CV) can be used to study the reduction and oxidation of molecular species.[18,19] This technique provides qualitative data on the electrode reaction mechanisms and quantitative data on charge transfer reactions between electrolytic ions and electrons at the electrode surface.[18]

This study investigated several electrodeposition parameters, such as the scan rate of CVs on three different gold substrates, to study the mass transport processes and reversibility systems. Additionally, the deposition current transients were investigated to understand the nucleation and growth mechanisms of the cobalt films on the three substrates. An important aspect of this study was to evaluate the use of gold substrates obtained from commercial compact discs (CDtrodes) because of their lower cost.

2. Experimental

2.1. Preparation of cobalt solution and substrates

Electrolytic solutions were prepared using high-purity chemicals (VETEC) and Milli-Q ultrapure water (resistivity of ~ 18.2 MΩ cm). The solution consisted of 1 mmol L^{-1} of H_2SO_4, 10 mmol L^{-1} of K_2SO_4 and 0.1 mmol L^{-1} of KCl. The pH was maintained at approximately 4, and $CoSO_4$ was added at a concentration of 1 mmol L^{-1}.[20]

The CDtrode substrates was prepared from commercial high-durability compact discs (CDs, Delkin Archival Gold Model). They have a gold layer in their structure with a nominal thickness of 50–100 nm, which can be exposed by removing the polymeric layers through chemical etching with a 58% solution of HNO_3 (VETEC), for 15 min.[22,23] After complete removal, the exposed gold layer was rinsed with distilled water and dried under an airflow. Figure 1 shows a representative scheme of the CDtrode preparation, from removing the polymeric layers to delineating the deposition area with varnish.

Au/Mica substrates were produced using a thermal evaporation technique with gold with high purity (99.9999%). Evaporation was performed on Mica discs (Metafix)with a diameter of 50 mm and thickness of approximately 0.1 mm, which were cleaved before deposition. The pressure in the deposition chamber was maintained at a vacuum of approximately 10^{-6} Torr, and the Mica was heated to approximately 350 °C, with a deposition rate between 0.3 and 0.4 nm s^{-1}, controlled by a quartz microbalance. Commercial Au/Silicon substrate (Stanford Advanced Materials) was used. The films were deposited using chemical vapor deposition (CVD) with a nominal thickness of 50 nm.

2.2. Preparation of cobalt thin films

The electrodeposition of Co thin films was carried out at room temperature in a cylindrical glass cell, using approximately 20 mL of the electrolyte solution. The classic potentiostatic technique was employed, consisting of an electrochemical cell with three electrodes in a triangular geometry to reduce the system's resistance and increase the current density.[20] A platinum wire was used as the counter electrode (CE), a silver wire as the quasi-reference electrode (RE), and the gold substrate as the working electrode (WE). A potentiostat (Autolab Model 302N) was used for control, with data collected using NOVA 1.9 software. The experimental setup is illustrated in Figure 2.

Cyclic voltammetry was used to identify the oxidation and reduction potentials of cobalt. Eight cyclic voltammetry

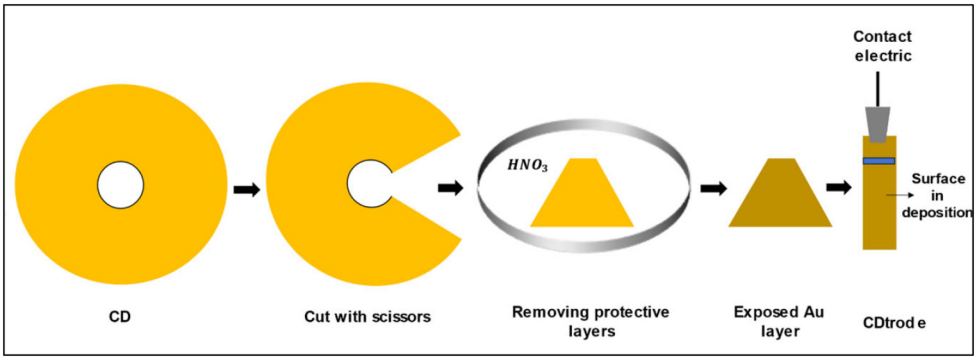

Figure 1. Schematic representation of CDtrode preparation

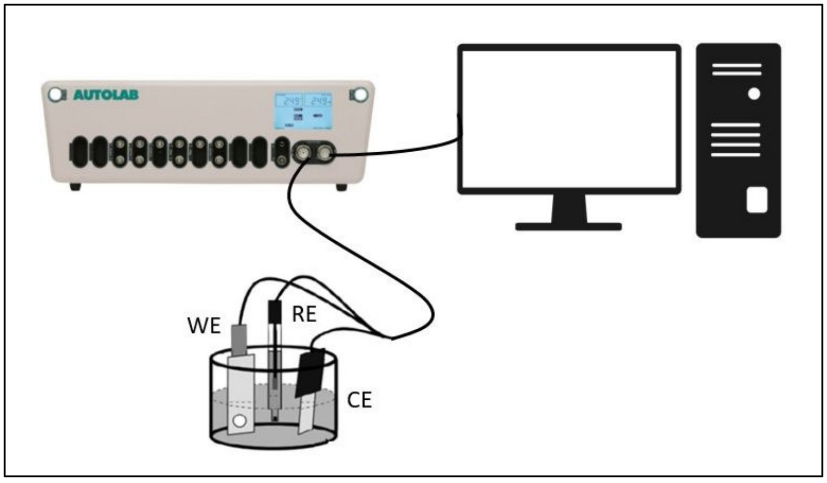

Figure 2. Schematic representation of the electroplating experimental electrodeposition

measurements were conducted at different scan rates for each substrate. The potential range used throughout the process was from 0.00 to -1.30 V. To evaluate the electrochemical activity in the electron transfer process on the different electrodes, the scan rates were set at 10, 20, 30, 50, 75, 100, 150, and 200 mV s^{-1}. To analyze the current transients, potentials of -0.90, -1.00, and -1.10 V were chosen for the electrode, -0.95, -1.05, and -1.15 V for Au/Mica, and -0.94, -1.04, and -1.14 V for Au/Si. The selected potentials were the reduction peak potential of cobalt and, 100 mV more negative, and 100 mV more positive.

2.3. Structural characterization

The structural quality of the gold substrates was determined using an X-ray diffractometer Ultima IV (RIGAKU) with Cu-Kα radiation (λKα = 1.5406 Å) in the 2θ range of 35-72°, in Bragg-Brentano geometry.

3. Results and Discussions

3.1. X-ray diffraction analysis

The gold substrates were subjected to X-ray diffraction to identify their crystallographic orientations. The diffraction pattern of CDtrode, Au/Mica, and Au/Silicon are presented in Figure 3 (3a-3c, respectively). The diffraction peak observed at 38.3° for all substrates corresponds to the cubic structure of metallic gold, with a preferential (111) crystallographic orientation. In Figure 3b, four other peaks were observed, centered at 36.0°, 45.4°, 55.2° and 65.4°, characteristic of muscovite mica. For the Au/Silicon substrate (Figure 3c), a peak at 69.9° was observed, corresponding to the silicon substrate, with a (400) crystallographic orientation.

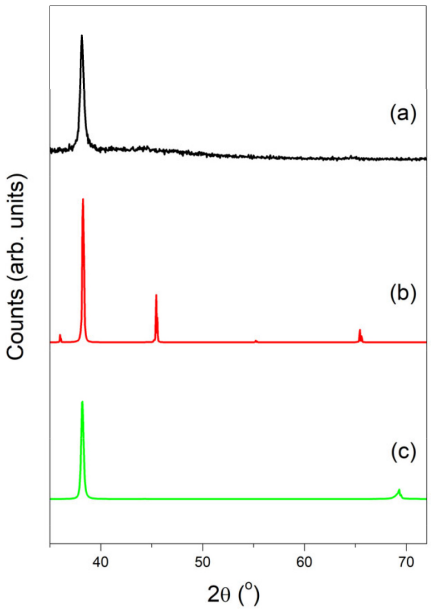

Figure 3. X-ray diffraction patterns of the (a) CDtrode substrate, (b) Au/Mica substrate, and (c) Au/Silicon substrate

3.2. Electrochemical characterization

To separately analyze the contributions of cobalt and hydrogen present in the CVs, experiments were conducted in an electrolytic solution composed of 1 mmol L^{-1} of H_2SO_4, 10 mmol L^{-1} of K_2SO_4, and 0.1 mmol L^{-1} of KCl. The potential range adopted was from 0.00 to –1.30 V, with a scan rate of 50 mV s^{-1}. Figure 4 presents the cyclic voltammograms of all substrates, with Figure 4a highlighting the voltammograms for CDtrode, Au/Mica, and Au/Si in the absence of cobalt, revealing that the reduction potential of hydrogen ions in solution ($H^+ + e^- \rightarrow 1/2H_2$) lies between –1.10 and –1.00 V for all substrates.

In Figure 4b, the cyclic voltammograms of the previous solution with the addition of 1 mmol L^{-1} of CoSO4 are shown for the different substrates, with a scan rate of 50 mV s^{-1}. A clear change in the cobalt deposition and dissolution area is observed for all substrates used in this study. The Au/Mica substrate exhibited higher catalytic activity (greater current density) compared to the other substrates. The cobalt reduction potential for all substrates is centered approximately between –1.10 and –1.20 V, corresponding to the reduction half-reaction ($Co^{2+} + 2e^- \leftrightarrow Co$).

The CV curves obtained for the CDtrode, Au/Mica, and Au/Silicon substrates in the cobalt metal solution at different

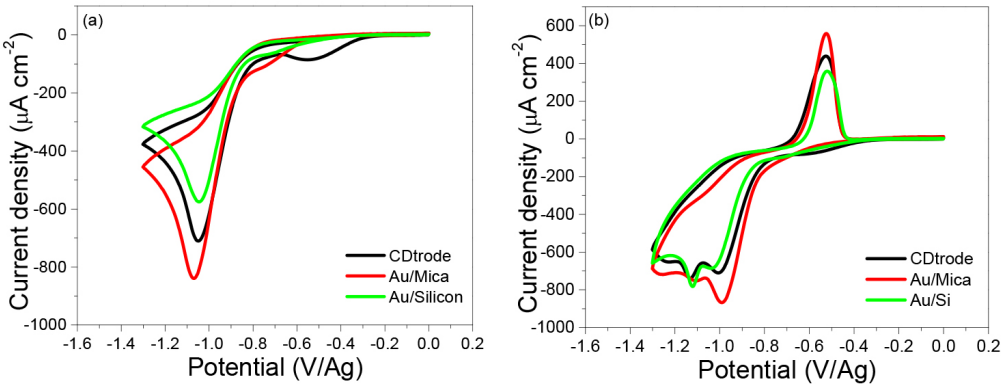

Figure 4. (a) Cyclic voltammetry for all substrates in a cobalt-free solution and (b) with the addition of cobalt

scan rates are shown Figure 5. From them, it can be observed that the hydrogen reduction potentials are located between –1.10 and –1.00 V for the CDtrode substrate, between –0.90 and –1.00 V for the Au/Mica system and centered at approximately –1.10 V for the Au/Silicon substrate. The cobalt deposition peak is approximately –1.20 V for the three substrates studied. The dissolution occurs between –0.90 and –0.40 V for the CDtrode substrate and between –0.80 and –0.40 V for the Au/Mica and Au/Silicon substrates.

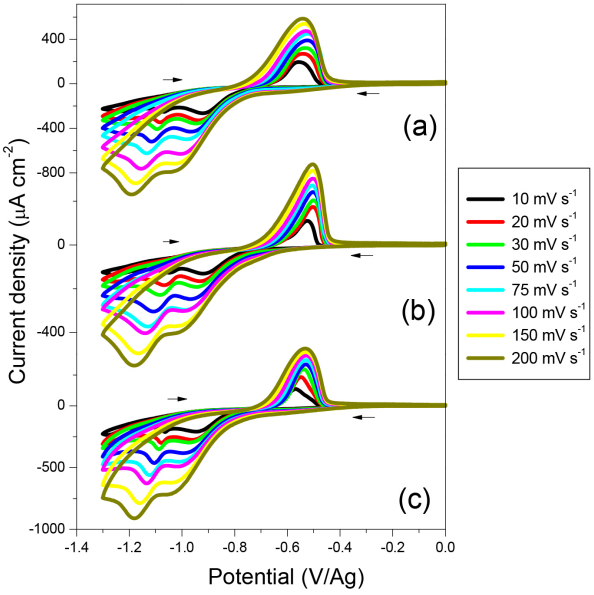

Figure 5. Cyclic voltammograms of the electrolytic solution containing 1 mmol L^{-1} of $CoSO_4$, at different scan rates for: (a) CDtrode, (b) Au/Mica and (c) Au/Silicon

The cyclic voltammograms presented in Figure 5 shows that as the scan rate increases, the peak currents of the electrochemical oxidation (I_{PA}) and reduction (I_{PC}) processes also increase. The redox peaks became sharper and the oxidation peak potential tended towards positive values, indicating that the reduction and oxidation reaction of cobalt was quasi-reversible.[24] As the scan rate increased, the oxidation process shifted to a more positive potential while the reduction process shifted to a more negative potential. It is also observed that the difference between the anodic and cathodic peak potentials (ΔE_p) increases as the scan rate is increased.

Based on the CVs presented in Figure 5, several parameters were obtained: the peak currents of the electrochemical oxidation (I_{PA}) and reduction (I_{PC}) processes, the ratio I_{PA}/I_{PC}, the potential of the cathodic peak current (E_{PC}), the potential of the anodic peak current (E_{PA}), and the separation between the anodic and cathodic peak potentials (Δ_{EP}), these values are summarized in Table 1.

The qualitative results obtained from the CV curves indicate that the cobalt oxidation process (film formation) is quasi-reversible, as the peak potential of the forward and reverse scans always move to different potential values. In contrast, for a reversible process they would present the same potential values (reduction and oxidation).[25] The CV curves for all electrodes showed areas of deposition and dissolution of the deposited cobalt thin films, which increased with increasing scan rate, indicating a direct proportional relationship between area and scan rate. The integrals of the oxidation and reduction processes, obtained from the CVs in Figure 5, are shown in Table 2.

The peak current values observed for all scan rates were consistently higher for the Au/Mica substrate. For example, by analyzing the peak current density at a scan rate of 200 mV s^{-1}, as shown in Table 1, it was observed that the current density during the reduction process on the Au/Mica substrate was approximately 11 and 36% higher than that of the CDtrode and Au/Silicon substrates, respectively. For the oxidation process, the current density on the Au/Mica substrate was 22 and 48% higher compared to the CDtrode and Au/Silicon substrates, respectively.

This increase suggests that the Au/Mica substrate has a lower electrical resistance, which may be attributed to an increase in the surface area, which can occur owing to the surface roughness as it alters the local electric field.[26] Therefore, the surface area plays an important role in the deposition and dissolution of the film. The current densities became more intense as the scan rate increased, owing to the effective formation of the double electric layer and rapid charge propagation on the electrodes.[27]

According to the experimental data obtained from the CV (Figure 5) and Table 1 the Au/Silicon substrate demonstrates a more reversible behavior than the CDtrode and Au/Mica substrates, as can be seen from the decrease in ΔE_P for Au/Silicon. This indicates a more reversible behavior of Au/Silicon than that of CDtrode and Au/Mica.[24]

To facilitate understanding of the behaviors of anodic and cathodic peak currents, graphs of I_{PA} and I_{PC} *versus* $v^{1/2}$ were plotted, as shown in Figure 6 along with linear regressions.

The values of the correlation coefficients *R* and the equations of the lines for the anodic and cathodic currents are listed in Table 3.

In the graphs shown in Figure 6, the anodic and cathodic peak currents show a linear dependence with the increase of the square root of the scan rate ($v^{1/2}$). This behavior suggests that the electrochemical reduction-oxidation processes of metallic cobalt are diffusion-controlled on all working electrodes, which is the determining step for the kinetics.[28,29] Correlation coefficients were equal to or greater than 0.950.

To evaluate the cobalt dissolution process, graphs of log I_{PA} *versus* log v were plotted for the CDtrode, Au/Mica, and Au/Silicon substrates, as shown in Figure 7. From the fits, the following angular coefficients were found: 0.358, 0.381, and 0.377 μA s mV^{-1}, for the CDtrode, Au/Mica, and Au/Silicon substrates, respectively. Based on these values, it can be concluded that the reactions are diffusion-controlled, because the slopes are close to 0.5, which is the theoretical value for diffusion-controlled systems.[23]

Table 1. Values of I_{PC}, I_{PA}, $I_{PA}/I_{PC,}$ E_{PC}, E_{PA}, and Δ_{Ep} for the CDtrode substrate

v (mV s^{-1})	I_{PC} (A)	I_{PA} (A)	I_{PA}/I_{PC}	E_{PC} (V)	E_{PA} (V)	ΔE_p (V)
CDtrode Substrate						
10	-175.9x10^{-6}	137.4x10^{-6}	0.781	-1.069	-0.557	0.512
20	-242.4x10^{-6}	188.8x10^{-6}	0.780	-1.084	-0.542	0.542
30	-284.2x10^{-6}	225.3x10^{-6}	0.792	-1.094	-0.532	0.562
50	-362.8x10^{-6}	272.8x10^{-6}	0.752	-1.116	-0.525	0.591
75	-436.6x10^{-6}	314.4x10^{-6}	0.720	-1.135	-0.522	0.613
100	-533.4x10^{-6}	331.4x10^{-6}	0.622	-1.154	-0.529	0.625
150	-625.0x10^{-6}	377.2x10^{-6}	0.603	-1.177	-0.535	0.642
200	-695.2x10^{-6}	409.6x10^{-6}	0.589	-1.194	-0.542	0.652
Au/Mica Substrate						
10	-180.3x10^{-6}	157.0x10^{-6}	0.872	-1.047	-0.525	0.522
20	-261.6x10^{-6}	247.8x10^{-6}	0.948	-1.067	-0.503	0.564
30	-325.4x10^{-6}	291.3x10^{-6}	0.896	-1.084	-0.500	0.584
50	-434.0x10^{-6}	344.9x10^{-6}	0.796	-1.108	-0.503	0.605
75	-531.7x10^{-6}	388.0x10^{-6}	0.729	-1.128	-0.505	0.623
100	-575.0x10^{-6}	432.1x10^{-6}	0.752	-1.140	-0.503	0.637
150	-707.4x10^{-6}	484.8x10^{-6}	0.686	-1.164	-0.503	0.661
200	-787.1x10^{-6}	526.8x10^{-6}	0.669	-1.181	-0.505	0.676
Au/Silicon Substrate						
10	-116.5x10^{-6}	74.62x10^{-6}	0.641	-1.064	-0.569	0.495
20	-165.3x10^{-6}	127.6x10^{-6}	0.772	-1.079	-0.549	0.530
30	-193.1x10^{-6}	162.9x10^{-6}	0.843	-1.089	-0.537	0.552
50	-254.8x10^{-6}	183.9x10^{-6}	0.722	-1.106	-0.529	0.577
75	-309.2x10^{-6}	203.8x10^{-6}	0.659	-1.123	-0.529	0.594
100	-345.6x10^{-6}	223.8x10^{-6}	0.647	-1.135	-0.529	0.606
150	-433.5x10^{-6}	239.3x10^{-6}	0.551	-1.159	-0.529	0.630
200	-501.1x10^{-6}	255.2x10^{-6}	0.509	-1.182	-0.532	0.650

Table 2. Integrals of the reduction (RI) and oxidation (OI) processes for all substrates

Scan Rate (mV s^{-1})	RI (V µA cm^{-2})	OI (V µA cm^{-2})	RI (V µA cm^{-2})	OI (V µA cm^{-2})	RI (V µA cm^{-2})	OI (V µA cm^{-2})
	CDtrode		Au/Mica		Au/Silicon	
10	-5.604x10^{-6}	4.683x10^{-6}	-8.066x10^{-6}	3.391x10^{-6}	-3.893x10^{-6}	1.994x10^{-6}
20	-1.094x10^{-5}	7.919x10^{-6}	-1.295x10^{-5}	5.987x10^{-6}	-7.021x10^{-6}	3.710x10^{-6}
30	-1.487x10^{-5}	1.136x10^{-5}	-1.725x10^{-5}	7.774x10^{-6}	-8.935x10^{-6}	5.070x10^{-6}
50	-2.537x10^{-5}	1.496x10^{-5}	-2.672x10^{-5}	9.874x10^{-6}	-1.626x10^{-5}	5.790x10^{-6}
75	-3.094x10^{-5}	1.892x10^{-5}	-3.679x10^{-5}	1.235x10^{-5}	-2.161x10^{-5}	7.521x10^{-6}
100	-4.765x10^{-5}	1.937x10^{-5}	-4.350x10^{-5}	1.492x10^{-5}	-2.902x10^{-5}	1.053x10^{-5}
150	-5.841x10^{-5}	2.469x10^{-5}	-5.328x10^{-5}	1.837x10^{-5}	-3.798x10^{-5}	1.235x10^{-5}
200	-7.783x10^{-5}	2.658x10^{-5}	-6.251x10^{-5}	2.080x10^{-5}	-4.822x10^{-5}	1.417x10^{-5}

To obtain more information to evaluate the degree of reversibility of the oxidation and reduction processes involved in the formation of the cobalt film on the studied substrates, the dependencies between the separation of the anodic and cathodic peak potentials (ΔE_P), the potential of the cathodic peak current (E_{PC}) and anodic peak current (E_{PA}), and the ratio I_{PA}/I_{PC} as a function of the scan rate were analyzed for CDtrode, Au/Mica, and (c) Au/Silicon (Figure 8). Figure 8a shows the plots of ΔE_P as a function of the scan rates, revealing similar behaviour among the three electrodes. As the scan rate increased, a corresponding rise in ΔEP was observed, which is characteristic of quasi-reversible electrochemical systems.[30] These results highlight the similar electrochemical performance of the three working electrodes, all exhibiting relatively high ΔE_P values. This behaviour points to a greater resistance—or

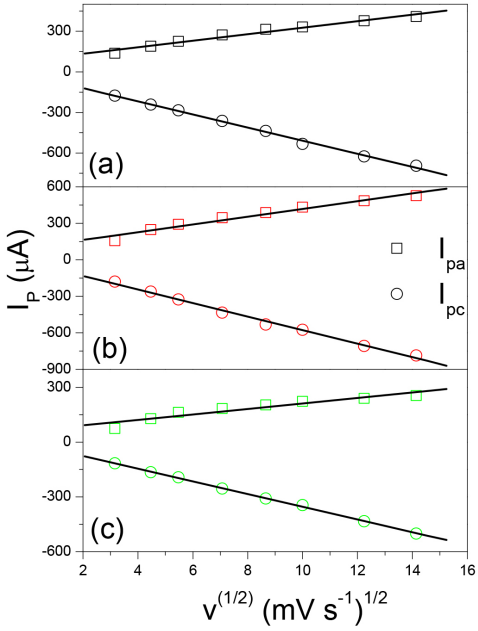

Figure 6. Plots of the experimental values of I_{PA} and I_{PC} as a function of $v^{1/2}$ (symbols) and their respective linear fits (lines) for the substrates: (a) CDtrode, (b) Au/Mica and (c) Au/Silicon

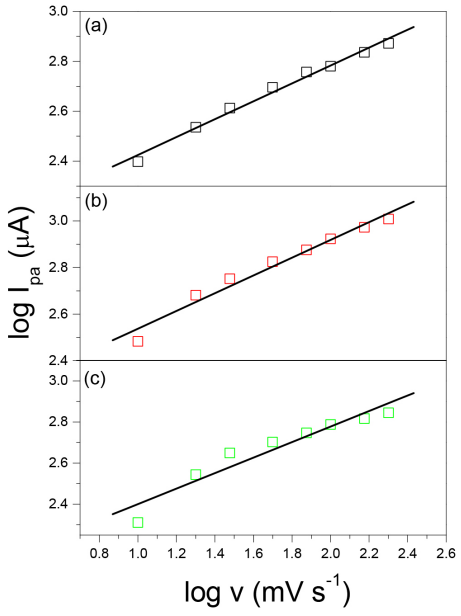

Figure 7. Plots of log I_{PA} *versus* log v and their respective fits for the substrates: (a) CDtrode, (b) Au/Mica, and (c) Au/Silicon

irreversibility—in ion transfer during redox processes occurring at the electrode–electrolyte interface, which in turn results in larger peak separations. Among the tested materials, the Au/Silicon electrode stood out by presenting improved reversibility compared to the other substrates, as evidenced by its lower ΔEP values.[31]

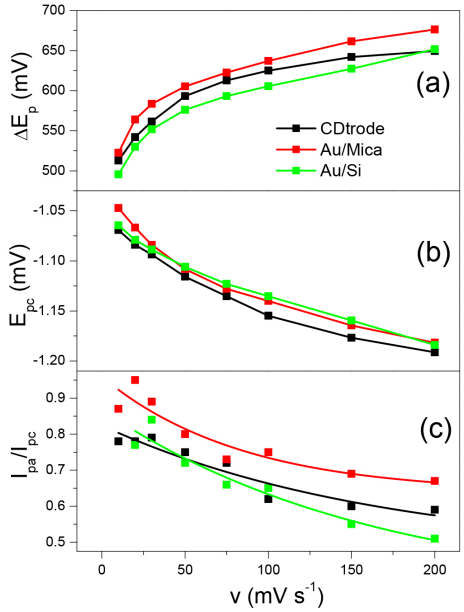

Figure 8. (a) Relationship between the separation of peak potentials (ΔE_P) and the scan rate (v). (b) Curve of E_{PC} for each substrate as a function of the scan rate. (c) I_{PA}/I_{PC} ratio as a function of the scan rate, with respective exponential fits

Another parameter used to study reversibility is E_{PC}. Plots of E_{PC} as a function of the scan rate for the three substrates (Figure 8b). These results show that both substrates exhibit curves typical of quasi-reversible processes. E_{PC} decreases with the scan rate v, in which case the current is controlled by mass transfer and charge transfer. Thus, it can be concluded that the scan rate influences the reversibility of both substrates.[32]

Analyzing the behavior of the I_{PA}/I_{PC} ratio as a function of the scan rate for cobalt (Figure 8c) and their respective fits, it can be noted that for all substrates, the I_{PA}/I_{PC} ratio decreases exponentially as v increases. Additionally, $I_{PA}/I_{PC} \neq 1$ for all peaks and scan rates. These characteristics are typical of quasi-reversible processes.[30,33]

3.3. Current transients *versus* time

To understand the nucleation and growth mechanism of the cobalt film on the three substrates, the cobalt films were deposited at a fixed time of 10 s at three different potentials, and the current and time data were recorded. The obtained

Table 3. Equations of the anodic and cathodic currents for the three studied systems and their respective correlation coefficients *R*

Substrate	Equation (Anodic Current)	*R*	Equation (Cathodic Current)	*R*
CDtrode	I_{PA}= 8.53x10^{-5}+2.41x10^{-5} v$^{1/2}$	0.986	I_{PC}= -2.37x10^{-5}–4.85x10^{-5} v$^{1/2}$	0.998
Au/Mica	I_{PA} = 9.94x10^{-5}+3.18x10^{-5} v$^{1/2}$	0.983	I_{PC} = -2.16x10^{-5}-5.56x10^{-5} v$^{1/2}$	0.997
Au/Silicon	I_{PA} = 6.16x10^{-5}+1.50x10^{-5} v$^{1/2}$	0.950	I_{PC} = -6.24x10^{-5}-3.48x10^{-5} v$^{1/2}$	0.999

transients are shown in Figure 9 (a-c) for the CDtrode, Au/Mica, and Au/Silicon substrates, respectively.

The nucleation peak in all the graphs demonstrates that the onset of the cobalt deposition process occurred at approximately 4 s, indicating the growth of cobalt on the substrate, followed by a slow decrease in the current until it stabilizes.

The transient curves demonstrate potential dependence for the Co/CDtrode and Co/Au/Silicon systems. Increasing the applied potential increases the current density, leading to a faster electrodeposition process. These curves are characteristic of three-dimensional nucleation growth processes under diffusion control.[34]

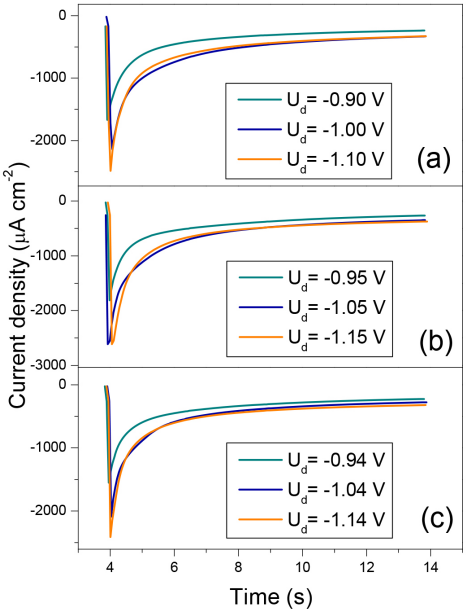

Figure 9. Deposition current transients of Co, for the substrates: (a) CDtrode using potentials of -0.90, -1.00, and -1.10 V, (b) Au/Mica using potentials of -0.95, -1.05, and -1.15 V and (c) Au/Silicon using potentials of -0.94, -1.04, and -1.14 V

The current transient curves for the Co/Au/Mica system (Figure 9b) show higher current densities, likely because the amount of cobalt II ions (Co^{2+}) to be consumed at the substrate/electrolyte interface allows for more active sites available for reduction, causing the deposition reaction of the reduction semi-reactions ($Co^{2+} + 2e^- \leftrightarrow Co$). In the Co/Au/Mica system, the nucleation peak of cobalt was observed at a current density of –2.613 μA cm^{-2}, which is higher than the current densities for the CDtrode (–2.486 μA cm^{-2}) and Au/Silicon (–2.411 μA cm^{-2}). The result confirms that the Au/Mica substrate provides more favorable conditions for the formation of nucleation sites and the consequent electrodeposition of cobalt.

4. Conclusions

In this study, we obtained high-quality, low-cost gold substrates (CDtrodes) and analyzed their electrochemical properties relative to other gold substrates. The qualitative CV results indicated that the cobalt´s oxidation and reduction processes were quasi-reversible for all working electrodes. Furthermore, the deposition and dissolution areas of the deposited cobalt thin films increased with increasing scan rate, indicating a direct proportional relationship between the area and scan rate.

The reduction and oxidation processes for the Au/Mica substrate showed higher current densities than those of the CDtrode and Au/Silicon, suggesting a lower electrical resistance for the Au/Mica electrode. This can also be attributed to increase substrate surface area, influenced by roughness, as it alters the local electric field. Therefore, the electrochemically active surface plays an important role in the deposition and dissolution of the film.

The CV plots showed that the Au/Silicon substrate demonstrated more reversible behavior than the CDtrode and Au/Mica substrates when analyzing the ΔE_P. The anodic and cathodic peak currents exhibited a linear dependence on the square root of the scan rate ($v^{1/2}$), and the angular coefficients of the log I_{PA} *versus* log v relationship were approximately 0.5. These behaviors suggest that the electrochemical processes of the reduction-oxidation of metallic cobalt are diffusion-controlled in all working electrodes.

The degree of reversibility of the oxidation and reduction processes involved in forming the cobalt film on the studied substrates was also confirmed. ΔE_P increased with the scan rates, E_{PC} decreased with the scan rate v, and the I_{PA}/I_{PC} ratio decreased exponentially as v increased. These parameters confirm that the behavior of the three electrodes was characteristic of quasi-reversible systems, and indicate that the reversibility of both substrates is influenced by v.

Acknowledgments

The authors are grateful for the support of the Conselho Nacional de Desenvolvimento Científico e Tecnológico (CNPq) (Universal grant # 426814/2018-5) and Coordenação de Aperfeiçoamento de Pessoal de Nível Superior – Brasil (CAPES) – Finance Code 001.

Conflict of Interest

The authors declare no conflict of interest.

Bibliographic References

1. Lee, O.; You, L.; Jang, J.; Subramanian, V.; Salahuddin, S.; Flexible spin-orbit torque devices. *Applied Physics Letters* **2015**, *107*, 252401. [Crossref]
2. Zhao, X.; Zhang, X.; Yang, H.; Cai, W.; Zhao, Y.; Wang, Z.; Zhao, W.; Ultra-efficient spin-orbit torque induced magnetic

switching in W/CoFeB/MgO structures. *Nanotechnology* **2019**, *30*, 335707. [Crossref]

3. Li, T.; Wang, Q.; Taallah, A.; Zhang, S.; Yu, T.; Zhang, Z.; Measurement of the magnetic properties of thin films based on the spin Hall effect of light. *Optics Express* **2020**, *28*, 29086. [Crossref]
4. Dziwoki, A.; Blyzniuk, B.; Freindl, K.; Madej, E.; Wilgocka-Ślęzak, D.; Korecki, J.; Spiridis, N.; Magnetic-Field-Assisted Molecular Beam Epitaxy: Engineering of Fe_3O_4 Ultrathin Films on MgO(111). *Materials* **2023**, *16*, 1485. [Crossref]
5. Aouassa, M.; Alhosaini, W.; Taha, T. A.; Magnetic Ge:Mn nanocrystals grown by MBE on insulator substrate for solar cell and photodetector applications. *Applied Surface Science* **2022**, *574*, 151644. [Crossref]
6. Wojciechowski, P.; Lewandowski, M.; Iron nitride thin films: Growth, structure, and properties. *Crystal Growth & Design* **2022**, *22*, 4618. [Crossref]
7. Li, T.; Liu, X.; Li, J.; Pan, L.; He, A.; Dong, Y.; Microstructure and magnetic properties of FeCoHfN thin films deposited by DC reactive sputtering. *Journal of Magnetism and Magnetic Materials* **2022**, *547*, 168777. [Crossref]
8. Gamez, J. D.; Martínez-Sánchez, H.; Valenzuela, J. L.; Marín, L.; Rodríguez, L. A.; Snoeck, E.; Zamora, L. E.; Pérez Alcázar, G. A.; Tabares, J. A.; Magnetic τ-MnAlC thin film fabrication by high-vacuum thermal evaporation. *Materials Letters* **2021**, *293*, 129657. [Crossref]
9. Shinde, K. P.; Sinha, B. B.; Oh, S. S.; Kim, H. S.; Ha, H. S.; Baik, S. K.; Chung, K. C.; Kim, D. S.; Jeong, S.; Fabrication of Gd films by vacuum evaporation and its magnetocaloric properties. *Journal of Magnetism and Magnetic Materials* **2015**, *374*, 144. [Crossref]
10. Oujja, M.; Martín-García, L.; Rebollar, E.; Quesada, A.; García, M. A.; Fernández, J. F.; Marco, J. F.; Figuera, J.; Castillejo, M.; Effect of wavelength, deposition temperature and substrate type on cobalt ferrite thin films grown by pulsed laser deposition. *Applied Surface Science* **2018**, *452*, 19. [Crossref]
11. Jameel, D. A.; Thin Film Deposition Processes. *International Journal of Modern Physics and Applications* **2015**, *1,* 193. [Crossref]
12. Karakovskaya, K. I.; Dorovskikh, S. I.; Vikulova, E. S.; Ilyin, I. Y.; Zherikova, K. V.; Basova, T. V.; Morozova, N. B.; Volatile Iridium and Platinum MOCVD Precursors: Chemistry, Thermal Properties, Materials and Prospects for Their Application in Medicine. *Coatings* **2021**, *11*, 78. [Crossref]
13. Yang, Y.; Tao, Q.; Srinivasan, G.; Takoudis, C. G.; Cyclic Chemical Vapor Deposition of Nickel Ferrite Thin Films Using Organometallic Precursor Combination. *ECS Journal of Solid State Science and Technology* **2014**, *3*, P345. [Crossref]
14. Oviroh, P. O.; Akbarzadeh, R.; Pan, D.; Coetzee, R. A. M.; Jen, T. C.; New development of atomic layer deposition: processes, methods and applications. *Science and Technology of Advanced Materials* **2019**, *20*, 465. [Crossref]
15. Hnida, K. E.; Marzec, M.; Wlaźlak, E.; Chlebda, D.; Szaciłowski, K.; Gilek, D.; Sulka, G. D.; Przybylski, M.; Influence of pulse frequency on physicochemical properties of InSb films obtained via electrodeposition. *Electrochimica Acta* **2019**, *304*, 396. [Crossref]
16. Rajska, D.; Motyka, K.; Kozieł, M.; Chlebda, D.; Brzózka, A.; Sulka, G. D.; Influence of synthesis parameters on composition and morphology of electrodeposited Zn-Sb thin films. *Journal of Industrial and Engineering Chemistry* **2020**, *84*, 202. [Crossref]
17. Balema, V. P.; Chemical Deposition Techniques in Materials Design. *Material Matters* **2006**, *1*, 3. [Crossref]
18. Navashree, N.; Parthasarathy, P.; A comparative study on electrochemical behaviour of various electrolytes by cyclic voltammetry: GCE as electrode material. *Materials Today: Proceedings* **2023.** [Crossref]
19. Dzulkurnain, N. A.; Mokhtar, M.; Rashid, J. I. A.; Knight, V. F.; Yunus, W. M. Z. W.; Ong, K. K.; Kasim, N. A. M.; Noor, S. A. M.; A Review on Impedimetric and Voltammetric Analysis Based on Polypyrrole Conducting Polymers for Electrochemical Sensing Applications. *Polymers* **2021**, *13*, 2728. [Crossref]
20. Battistel, A.; Fan, M.; Stojadinović, J.; La Mantia, F.; Analysis and mitigation of the artefacts in electrochemical impedance spectroscopy due to three-electrode geometry. *Electrochimica Acta* **2014**, *135*, 133. [Crossref]
21. Gündel, A.; Cagnon, L.; Gomes, C. I.; Morrone, A.; Schmidt, J.; Allongue, P.; *In-situ* magnetic measurements of electrodeposited ultrathin Co, Ni and Fe/Au(111) layers. *Physical Chemistry Chemical Physics* **2001**, *3*, 3330. [Crossref]
22. Foguel, M. V.; Santos, G. P.; Ferreira, A. A. P.; Magnani, M.; Mascini, M.; Skladal, P.; Benedetti, A. V.; Yamanaka, H.; Comparison of Gold CD-R Types as Electrochemical Device and as Platform for Biosensors. *Journal of the Brazilian Chemical Society* **2016**, *27*, 650. [Crossref]
23. Richter, E. M.; Augelli, M. A.; Kume, G. H.; Mioshi, R. N.; Angnes, L.; Gold electrodes from recordable CDs for mercury quantification by flow injection analysis. *Fresenius' Journal of Analytical Chemistry* **2000**, *366*, 444. [Crossref]
24. Askari, N.; Salarizadeh, N.; Askari, M. B.; Electrochemical determination of rutin by using $NiFe_2O_4$ nanoparticles-loaded reduced graphene oxide. *Journal of Materials Science: Materials in Electronics* 2**021**, *32*, 9765. [Crossref]
25. Fontanesi, C.; Como, E. D.; Vanossi, D.; Montecchi, M.; Cannio, M.; Mondal, P. C.; Giurlani, W.; Innocenti, M.; Pasquali, L.; Redox-Active Ferrocene grafted on H-Terminated Si(111): Electrochemical Characterization of the Charge Transport Mechanism and Dynamics. *Scientific Reports* **2019**, *9*, 8735. [Crossref]
26. Liu, Q.; Yang, J.; Wang, R.; Wang, H.; Ji, S.; Manganese dioxide core–shell nanostructure to achieve excellent cycling stability for asymmetric supercapacitor applications. *RSC Advances* **2017**, *53*, 33635. [Crossref]
27. Nady, J. E. L.; Shokry, A.; Khalil, M.; Ebrahim, S.; Elshaer, A. M.; Anas, M.; One-step electrodeposition of a polypyrrole/NiO nanocomposite as a supercapacitor electrode. *Scientific Reports* **2022**, *12*, 3611. [Crossref]
28. Munteanu, I. G.; Grădinaru, V. R.; Apetrei, C.; Development of a Chemically Modified Sensor Based on a Pentapeptide and Its Application for Sensitive Detection of Verbascoside in Extra Virgin Olive Oil. *International Journal of Molecular Sciences* **2022**, *23*, 15704. [Crossref]

29. Munteanu, I. G.; Apetrei, C.; Electrochemical Determination of Chlorogenic Acid in Nutraceuticals Using Voltammetric Sensors Based on Screen-Printed Carbon Electrode Modified with Graphene and Gold Nanoparticles. *International Journal of Molecular Sciences* **2021**, *22*, 8897. [Crossref]
30. Greef, R.; Peat, R.; Peter, L. M.; Pletcher, D.; Robinson, J.; *Instrumental Methods in Electrochemistry,* 1a. ed., Ellis Horwood Ltd: Chichester, 1985.
31. Stefano, J. S.; Silva, L. R. G.; Rocha, R. G.; Brazaca, L. C.; Richter, E. M.; Muñoz, R. A. A.; Janegitz, B. C.; New conductive filament ready-to-use for 3D-printing electrochemical (bio) sensors: Towards the detection of SARS-CoV-2. *Analytica Chimica Acta* **2022**, *1191*, 339372 [Crossref]
32. Zanello, P.; *Inorganic Electrochemistry, Theory, Practice and Application*. 1a. ed., The Royal Society of Chemistry: Cambridge, **2003**.
33. Brett, A. M. O.; Brett, C. M. A.; *Electrochemistry: Principles, Methods, and Applications*. 1a. ed., Oxford Science Publication: Oxford, **1996**.
34. Hamla, M.; Derbal, S.; Dilmi, O.; Allam, M.; Benaicha, M.; Electrochemical Nucleation and Growth of Copper–Tin Alloys from Ammonia-Free Citrate-Based Electrolyte. *Arabian Journal for Science and Engineering* **2023**, *48,* 7543. [Crossref]